

Order in de Broglie - Bohm quantum mechanics

G. Contopoulos, N.Delis and C. Efthymiopoulos

Research Center for Astronomy and Applied Mathematics, Academy of Athens,
Soranou Efessiou 4, 11527 Athens, Greece

E-mail: gcontop@academyofathens.gr, nikdelis@sch.gr,
cefthim@academyofathens.gr

Abstract. A usual assumption in the so-called *de Broglie - Bohm* approach to quantum dynamics is that the quantum trajectories subject to typical ‘guiding’ wavefunctions turn to be quite irregular, i.e. *chaotic* (in the dynamical systems’ sense). In the present paper, we consider mainly cases in which the quantum trajectories are *ordered*, i.e. they have zero Lyapunov characteristic numbers. We use perturbative methods to establish the existence of such trajectories from a theoretical point of view, while we analyze their properties via numerical experiments. Using a 2D harmonic oscillator system, we first establish conditions under which a trajectory can be shown to avoid close encounters with a moving nodal point, thus avoiding the source of chaos in this system. We then consider series expansions for trajectories both in the interior and the exterior of the domain covered by nodal lines, probing the domain of convergence as well as how successful the series are in comparison with numerical computations or regular trajectories. We then examine a Hénon - Heiles system possessing regular trajectories, thus generalizing previous results. Finally, we explore a key issue of physical interest in the context of the de Broglie - Bohm formalism, namely the influence of order in the so-called *quantum relaxation* effect. We show that the existence of regular trajectories poses restrictions to the quantum relaxation process, and we give examples in which the relaxation is suppressed even when we consider initial ensembles of only chaotic trajectories, provided, however, that the system as a whole is characterized by a certain degree of order.

PACS numbers: 03.65.-w – 03.65.Ta

1. Introduction

The de Broglie - Bohm version of quantum mechanics [11][2][4][27][16] considers trajectories guided by the wave function, which is a solution of Schrödinger's equation, i.e. (in the one particle case)

$$\left(-\frac{1}{2}\nabla^2 + V\right)\psi = i\frac{\partial\psi}{\partial t} \quad (1)$$

where V is the potential and we have set $m = \hbar = 1$. The de Broglie - Bohm mechanics gives results which are equivalent to the Copenhagen version of quantum mechanics. However it gives further information about the trajectories of particles, or fluid elements of a probabilistic fluid, given by the probability $p = |\psi|^2$ [30]. The de Broglie - Bohm equations of motion are

$$\frac{d\vec{r}}{dt} = \text{Im}\left(\frac{\nabla\psi}{\psi}\right) . \quad (2)$$

The quantum trajectories are either ordered or chaotic. The problem of chaos in the de Broglie - Bohm theory has been studied extensively (indicative references are [15][21][33][24] [13][28][23][29] [44][31][10][12] [22][45][46][38]). In four previous papers [18][19][8] [20] we studied in detail the basic mechanism by which chaos is generated when the trajectories come close to *nodal points*, where $\psi = 0$. The appearance of *quantum vortices* at nodal points is a well known phenomenon [14], which, besides chaos, leads to a number of interesting consequences for quantum dynamics in general (e.g. [32][25] [26][36][37]). Quantitative studies of chaos related to the effects of vortices are presented in [23][38] [20]. The fact that the generation of chaos is due to the *motion* of quantum vortices was first pointed out in [45](see also [46]). Our own main result was to show that chaos is due to the formation (by moving nodal points) of 'nodal point - X-point complexes' [19][8][20]. More specifically, we found that near every nodal point there is a hyperbolic point, called X-point, that has two unstable directions, opposite to each other, and two stable directions, again opposite to each other. Chaos is introduced when a trajectory approaches such an X-point. Furthermore chaos is stronger when the X-point is closer to the nodal point. As shown in [20], the existence of an X-point close to a nodal point is a consequence of the topological properties of the quantum flow holding in the neighborhood of nodal points for an arbitrary form of the wavefunction. Furthermore, we made a theoretical analysis of the dependence of the Lyapunov characteristic numbers of the quantum trajectories on the size and speed of the quantum vortices. Roughly, the local value of Lyapunov characteristic numbers scales inversely proportionally to the distance of a quantum trajectory from the stable manifold of the X-point, and to the speed of the nodal point. Furthermore, the size of the nodal point - X-point complex scales inversely proportionally to the speed of the nodal point. These properties were used to estimate how close a trajectory must approach the X-point for chaos to become effective, thus explaining numerical results found in [19] and [8].

On the other hand trajectories that never approach a "nodal point - X point complex" are ordered. Such trajectories were considered in [19] (called hereafter EKC). In that paper we found the trajectories and the nodal lines (i.e. the lines formed by moving nodal points) in the case of a simple model of a 2D harmonic oscillator, when one considers a superposition of three eigenfunctions. Other examples of ordered orbits, following a similar analysis, were given in [20].

In EKC we found the forms of the nodal lines and some limiting curves that are never crossed by the nodal lines. In fact we found that the nodal lines never come (a) close to the center or close to the axis $x = 0$ (b) close to the axis $y = 0$ for large absolute values of x , and (c) large values of both x and y . This is exemplified in Fig.1a,b, referring to an example of trajectory calculations taken from EKC (see section 2 below for details). The main effect to be noted is that there are empty regions left by the nodal lines. As shown in EKC and in [20], the appearance of order is due to the presence of such regions devoid of nodal points at all times t . Further examples in a different (square-box) model were given in [9].

The most notable physical consequence of the existence of regular trajectories is related to a phenomenon called *quantum relaxation* [40][43]. If we allow the initial conditions of the Bohmian particles to obey a probability distribution $p_0 \neq |\psi_0|^2$, where ψ_0 is the initial wavefunction, then, under some conditions we find that p_t approaches $|\psi_t|^2$ asymptotically, at a coarse-grained level, as the time t increases. The possibility to obtain an asymptotic approach of p to $|\psi|^2$ due to stochastic fluctuations of the motion of the probabilistic fluid elements was first pointed out by Bohm and Vigier [3]. However, the theory of Valentini [40] does not rely on extra assumptions besides the absence of the so-called micro-state fine structure in the initial distribution of the particles. Quantum relaxation has been observed in a number of numerical simulations ([43][18][39]). The main condition for its effectiveness, however, is that the trajectories considered must be *chaotic*. In fact, it is known that the existence of ordered trajectories limits the effectiveness of quantum relaxation [18].

Since the physics of quantum relaxation has attracted recent interest in a variety of physical contexts (e.g. [1][6][42]), it is important to understand, besides the mechanisms of chaos, also the mechanisms by which order appears in de Broglie - Bohm mechanics. This is our purpose in the present paper.

The paper is organized as follows: In section 2, we consider inner ordered trajectories, i.e. ordered trajectories appearing in the central region of the configuration space of the same model as in EKC. In particular, using perturbation series we explain why there can be some ordered trajectories partly overlapping with the domain covered by nodal lines in this model. In section 3 we discuss the issue of convergence of the perturbation series representing the regular trajectories. Section 4 deals with ordered trajectories far from the center, i.e. beyond the domain covered by nodal lines. In section 5 we discuss ordered trajectories in a more general (Hénon - Heiles) model than the 2D harmonic oscillator. Section 6 deals with the impact of order on the effect of quantum relaxation, while section 7 discusses further examples and some quantitative

analysis of the same subject. Finally, section 8 presents the main conclusions of the present study.

2. Inner ordered trajectories

In EKC we considered the Bohmian trajectories in the 2D harmonic oscillator model:

$$H = \frac{1}{2}(p_x^2 + p_y^2) + \frac{1}{2}(x^2 + (cy)^2) \quad (3)$$

when the guiding field is the superposition of the ground state and the two first excited states

$$\psi(x, y, t) = e^{-\frac{x^2+cy^2}{2}-i\frac{(1+c)t}{2}}(1 + axe^{-it} + bc^{1/2}xye^{-i(1+c)t}) \quad (4)$$

with real amplitudes a, b and incommensurable frequencies $\omega_1 = 1$, $\omega_2 = c$. The equations of motion are:

$$\begin{aligned} \frac{dx}{dt} &= -\frac{a \sin t + bc^{1/2}y \sin(1+c)t}{G} \\ \frac{dy}{dt} &= -\frac{bc^{1/2}x(ax \sin ct + \sin(1+c)t)}{G} \end{aligned} \quad (5)$$

where

$$G = 1 + a^2x^2 + b^2cx^2y^2 + 2ax \cos t + 2bc^{1/2}xy \cos(1+c)t + 2abc^{1/2}x^2y \cos ct \quad (6)$$

As shown in EKC, the domains covered by the nodal lines are hyperbola-like, leaving both inner and outer domains devoid of nodal points. The nodal points are at

$$x_N = -\frac{\sin(1+c)t}{a \sin ct}, \quad y_N = -\frac{a \sin t}{bc^{1/2} \sin(1+c)t} \quad (7)$$

Trajectories that never approach the ‘nodal point - X point complex’ are ordered. Such trajectories were found in EKC both numerically and by analytical expansions. We can explicitly show that whether an orbit is regular or chaotic depends on how close the orbit can come to the nodal point. Furthermore, we find that almost symmetric initial conditions can give rise to quite different trajectories (ordered or chaotic), because the overlapping of the initial conditions with the domain of the nodal lines does not guarantee that there is a close encounter (in both space and time) of the trajectories with the nodal point.

As an example, trajectories starting on the upper right quadrant are regular, even if their initial conditions are located in a region occupied by the nodal lines (Fig.1a, case $x_0 = y_0 = 1$), while trajectories starting in the lower left region occupied by the nodal lines are chaotic (Fig.1b, case $x_0 = y_0 = -1$). The reason for this difference is that, when the moving point is close to its maximum (x and y), it can be shown that the nodal point is always far from the moving point in the first case ($x_0 = y_0 = 1$), while it comes several times close to it in the second case ($x_0 = y_0 = -1$). A rough estimate of the position of the moving point can be given by a first order theory. Namely, from Eqs.(5) we derive up to first order in a, b :

$$x = x_0 + a(\cos t - 1) + \frac{bc^{1/2}y_0}{1+c} \left(\cos(1+c)t - 1 \right) + \dots \quad (8)$$

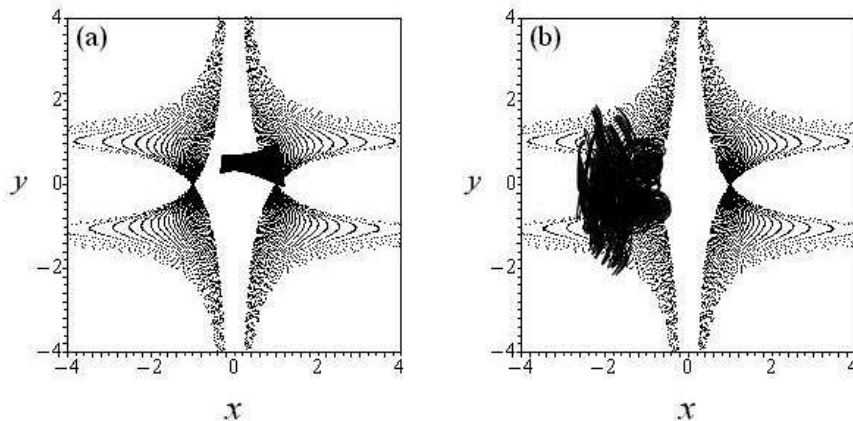


Figure 1. Bohmian trajectories in a 2D harmonic oscillator model when the wavefunction ψ is a superposition of three states (Eq.(4)), and $a = b = 1$, $c = \sqrt{2}/2$. (a) An ordered trajectory with $x_0 = y_0 = 1$, and (b) a chaotic trajectory with $x_0 = y_0 = -1$. In the background we mark the nodal lines, i.e. the solutions for x, y of the equation $\psi(x, y, t) = 0$.

$$y = y_0 + \frac{bc^{1/2}x_0}{1+c} \left(\cos(1+c)t - 1 \right) + \dots \quad (9)$$

These expressions are found in practice to be fairly accurate well beyond the domain (in a, b) where the convergence of the series representing x or y can be rigorously established (see section 3 below), and for initial conditions x_0, y_0 satisfying $|x_0 y_0| < 1/(bc^{1/2})$ (see EKC). Using the approximate expression (8), we find that we have a maximum $x = x_0$ when

$$a \sin t + bc^{1/2}y_0 \sin(1+c)t = 0, \quad (10)$$

provided that the time t specified by (10) satisfies the inequality

$$a \cos t + bc^{1/2}y_0(1+c) \cos(1+c)t > 0. \quad (11)$$

Equation (10) gives the times of the maximum x . If the quantity

$$q = \frac{bc^{1/2}}{a}y_0 \quad (12)$$

is relatively small (e.g. $|q| \leq 0.5$) the times of maximum t are close to $2K\pi$ for some integer K . Then, we can write

$$t = 2K\pi + t' \quad (13)$$

with

$$\sin t = \sin t' \approx -q \sin[(1+c)2K\pi] = -q \sin(c2K\pi) \quad (14)$$

and the inequality (11) is satisfied.

At such a time the nodal point is near the position

$$x_N = -\frac{\sin(1+c)t}{a \sin ct} = \frac{\sin t}{qa \sin ct} \approx -\frac{1}{a} \quad (15)$$

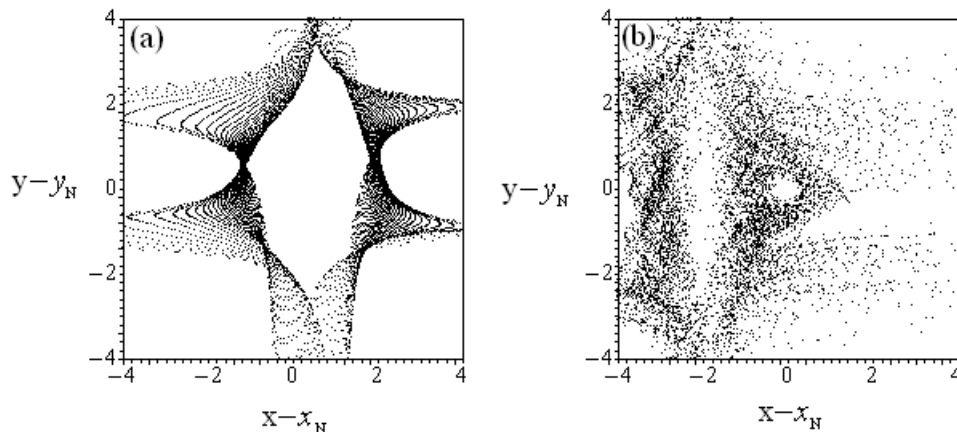


Figure 2. Distribution of the quantities $x(t) - x_N(t)$, $y(t) - y_N(t)$, where $x(t), y(t)$ are a trajectory's coordinates and $x_N(t), y_N(t)$ are the nodal point coordinates at various times t , (a) for the ordered trajectory, and (b) for the chaotic trajectory of Fig.1.

$$y_N = -\frac{a \sin t}{bc^{1/2} \sin(1+c)t} \approx y_0 \quad (16)$$

Therefore when x is at its maximum the nodal point is at a negative x_N . Thus if $x_0 > 0$, $y_0 > 0$ the moving point is in the upper right quadrant, while the nodal point (x_N, y_N) is in the upper left quadrant, i.e. far from the moving point. On the other hand if $x_0 < 0$, $y_0 < 0$ the moving point at its maximum x is in the lower left quadrant, and the nodal point is also in the lower left quadrant, therefore the two points can be close and this closeness introduces chaos.

The difference between the ordered case $x_0 = y_0 = 1$ and the chaotic case $x_0 = y_0 = -1$ can be seen in Figs.2a,b where we give the points ($u = x_0 - x_N$, $v = y_0 - y_N$) whenever the distance $d_N = \sqrt{u^2 + v^2}$ goes through a local minimum in time. In this figure the nodal point is at $u_N = v_N = 0$. We see that in the first case the local minima d_N in time never approach the value 0, while in the second case d_N sometimes approaches zero. This explains why the first trajectory is ordered, while the second trajectory is chaotic.

3. Series convergence

The series representing regular orbits can be convergent only within a certain domain in the space of parameters (a, b in the case of the model (4)), and/or in the initial conditions x_0, y_0 . However, in some simple cases we can show that there are regular orbits even beyond the domains of convergence of the series constructed to represent such orbits.

One such example is found when $b = 0$. In this case all the trajectories in the model (4) are periodic, with period $T = 2\pi$, thus they are regular. Such trajectories

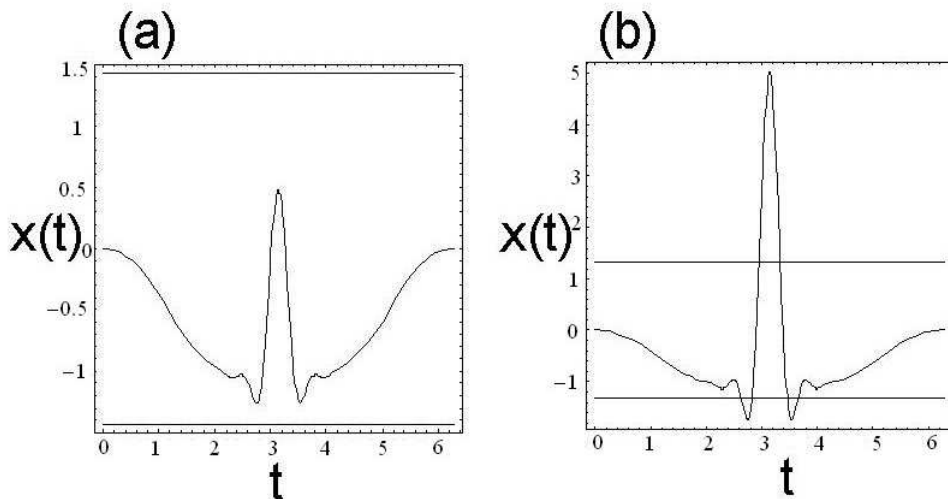


Figure 3. The time evolution of $x(t)$ in a series representation (truncated at order 20) of the trajectory with initial conditions $x_0 = y_0 = 0$ when $c = \sqrt{2}/2$, $b = 0$ and (a) $a = 0.7$, (b) $a = 0.75$. The two horizontal lines in each plot mark the interval of convergence of the series in the x -axis. The crossing of these lines by the series solution for $x(t)$ indicates that the series are divergent.

were considered in [8]. The equations of motion take a simple form:

$$\frac{dx}{dt} = -\frac{a \sin t}{1 + a^2 x^2 + 2ax \cos t}, \quad \frac{dy}{dt} = 0 \quad . \quad (17)$$

Thus, all the trajectories are straight horizontal lines, i.e. $y(t) = y_0 = \text{const.}$

Now, a series representation for the solution $x(t)$ can be obtained as a limiting case of the expansion considered in section 2. We set $x(t) = x_0 + x_1(t) + x_2(t) + \dots$, where $x_k(t)$ is of order k in the parameter a . For any fixed value of x, t , such a series is valid in the domain of analyticity of the function appearing in the r.h.s. of Eq.(17) with respect to a (considered as a complex variable). The latter domain can be determined by finding the nearest pole (with respect to the origin) of the function $1/G$, where $G = 1 + a^2 x^2 + 2ax \cos t$. For fixed (x, t) , the solution of $G = 0$ is

$$a = \frac{-\cos t \pm i|\sin t|}{x} \quad (18)$$

Thus the nearest pole is at the distance $|a| = 1/|x|$ for all times t .

The latter property allows for an easy numerical convergence test of the series representing $x(t)$. I.e., for a fixed value of a , we compute a finite truncation

$$x(t) \simeq x_0 + \sum_{k=1}^N x_k(t) \quad (19)$$

where N is a (finite) truncation order, and check whether the numerically computed values of $x(t)$ by the above expression ever cross the limit $|x(t)a| < 1$ in the interval $0 \leq t < 2\pi$. Figure 3 shows this criterion, when $x_0 = 0$, $N = 20$, and a is given two different values, namely $a = 0.7$ (Fig.3a) and $a = 0.75$ (Fig.3b). The horizontal straight lines correspond to the limit $|x(t)a| = 1$. The crossing of this limit takes place a little

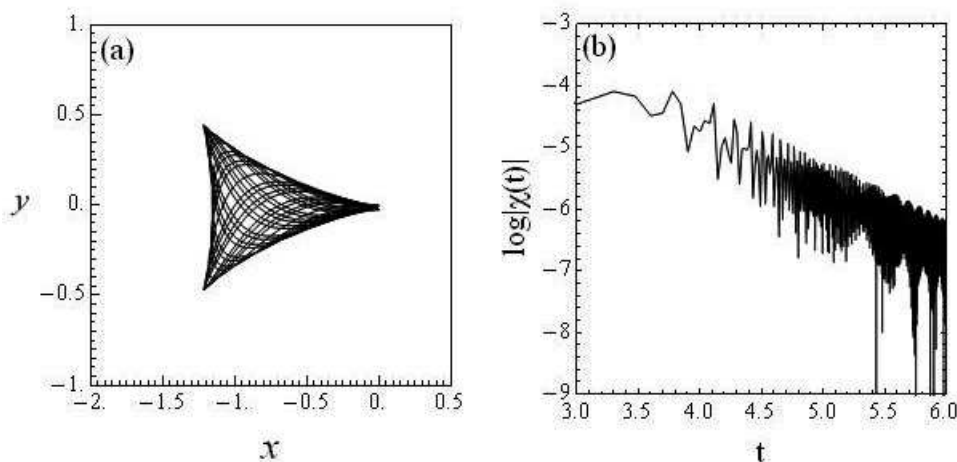


Figure 4. (a) A trajectory when $a = b = 0.75$, $c = \sqrt{2}/2$, and $x_0 = y_0 = 0$. (b) The time evolution of the ‘Finite time Lyapunov Characteristic Number’ $\chi(t)$ (see text) for the same trajectory, up to the time $t = 10^6$. The asymptotic logarithmic slope is -1 , indicating that the trajectory is regular.

beyond $a = 0.7$, thus we conclude that the series representing periodic trajectories are divergent beyond this value of a . It should be stressed, however, that the fact that the series are divergent only implies that the method used to compute these series no longer yields a useful representation of the true trajectories, since, in fact, the true trajectories *are* regular (because they are periodic).

The same effect is found when $b \neq 0$, i.e. we can establish the existence of regular orbits by numerical means even when the series constructed to represent them are divergent. In such cases, a low order truncation of the series is often found to continue to represent some features of the true orbits.

The regular character of the trajectories can be established numerically by computing their Lyapunov characteristic numbers. Such a test is shown in Figure 4, referring to a trajectory in the model (4) for $a = b = 0.75$, $c = \sqrt{2}/2$ and initial conditions $x_0 = y_0 = 0$. This trajectory was considered in [8] (Fig.12c,d of that paper), and it was found that the series representation of the trajectory clearly diverges. In order to check whether the trajectory’s character remains regular over longer time intervals, we computed the same trajectory, along with its variational equations, with a very precise time step $\Delta t = 10^{-5}$ up to a time $t = 10^6$. Figure 4b shows the evolution of the ‘finite time Lyapunov characteristic number’

$$\chi(t) = \frac{1}{t} \ln \left| \frac{\xi(t)}{\xi(0)} \right| \quad (20)$$

for this trajectory, where $\xi(t)$ is the length of a deviation vector computed from the variational equations of motion. The Lyapunov characteristic number is the limit $LCN = \lim_{t \rightarrow \infty} \chi(t)$. This limit is positive for chaotic trajectories, while it is zero for regular trajectories, for which $\chi(t)$ follows the asymptotic behavior $\chi(t) \sim t^{-1}$. This is

exactly the average power law found in the case of Fig.4b. Thus, all numerical indications are that this particular trajectory is regular, i.e. the domain of initial conditions and parameters leading to regular trajectories extends beyond the rigorous lower bounds provided by perturbation theory.

4. Ordered trajectories far from the center

Trajectories restricted far from the nodal lines are ordered. For the trajectories starting in the upper right domain beyond the set of nodal lines, and close to the diagonal, the initial conditions x_0, y_0 are both absolutely large. Therefore, $1/x_0, 1/y_0$ are small. We then set

$$X(t) = \frac{1}{x_0}x(t), \quad Y(t) = \frac{1}{y_0}y(t) \quad (21)$$

whereby it follows that $X(0) = Y(0) = 1$. Assuming that the trajectories only make small oscillations around the values $X = Y = 1$, we may write expansions of the form

$$X(t) = 1 + X_1(t) + X_2(t) + \dots, \quad Y(t) = 1 + Y_1(t) + Y_2(t) + \dots \quad (22)$$

in which we require that the quantities $X_j(t), Y_j(t)$ contain only terms with coefficients $(x_0^k y_0^l)^{-1}$ satisfying $k + l = j$, and $X_j(0) = Y_j(0) = 0$.

Upon substitution of (22) into (5), where, in addition, $x = x_0 X, y = y_0 Y$, the equations of motion for X, Y split into terms of like orders j . In the first and second orders we find the trivial equations

$$\frac{dX_1}{dt} = \frac{dY_1}{dt} = 0, \quad \frac{dX_2}{dt} = \frac{dY_2}{dt} = 0 \quad (23)$$

from which the solutions $X_1 = Y_1 = X_2 = Y_2 = 0$ are selected. The third and fourth order equations read

$$\frac{dX_3}{dt} = 0, \quad \frac{dY_3}{dt} = \frac{-a \sin ct}{bc^{1/2}y_0^3} \quad (24)$$

with solution

$$X_3(t) = 0, \quad Y_3(t) = \frac{a(\cos ct - 1)}{bc^{3/2}y_0^3}, \quad (25)$$

and

$$\frac{dX_4}{dt} = \frac{-\sin(1+c)t}{bc^{1/2}x_0^3y_0}, \quad \frac{dY_4}{dt} = \frac{a^2 \sin 2ct}{b^2cy_0^4} - \frac{\sin(1+c)t}{bc^{1/2}x_0y_0^3} \quad (26)$$

with solution

$$X_4 = \frac{\cos(1+c)t - 1}{bc^{1/2}(1+c)x_0^3y_0}, \quad Y_4 = \frac{-a^2(\cos 2ct - 1)}{2b^2c^2y_0^4} + \frac{\cos(1+c)t - 1}{bc^{1/2}(1+c)x_0y_0^3} \quad (27)$$

respectively. Higher order terms can be found by implementing the recursive scheme.

We checked the approximation of the numerical trajectories, when $a = b = 1$ and $c = \sqrt{2}/2$, by the series expansions (22) calculated up to order 15 via a computer algebraic program, We find that for x_0, y_0 large enough the approximation is excellent. However, as we decrease x_0 or y_0 the deviations between the analytical and numerical

| $x_0 = y_0$ | 4th approximation | | 15th approximation | | numerical | |
|-------------|-------------------|-----------------|--------------------|-----------------|-----------------|-----------------|
| | x_{min}^{max} | y_{min}^{max} | x_{min}^{max} | y_{min}^{max} | x_{min}^{max} | y_{min}^{max} |
| 3.4 | 3.4 | 3.4 | 3.412 | 3.4 | 3.412 | 3.4 |
| | 3.365 | 3.074 | 3.354 | 2.996 | 3.353 | 2.994 |
| 3.2 | 3.2 | 3.2 | 3.215 | 3.2 | 3.216 | 3.2 |
| | 3.158 | 2.830 | 3.146 | 2.715 | 3.139 | 2.707 |
| 3.0 | 3.0 | 3.0 | 3.021 | 3.0 | 3.022 | 3.0 |
| | 2.948 | 2.576 | 2.920 | 2.398 | 2.914 | 2.366 |
| 2.8 | 2.8 | 2.8 | 2.830 | 2.8 | 2.869 | 2.8 |
| | 2.737 | 2.309 | 2.687 | 2.016 | 2.616 | 1.452 |

Table 1. The minimum and maximum values of x and y for some ordered orbits far from the center (initial conditions $x_0 = y_0$ as indicated in the first column), using a series representation (Eq.22) up to the fourth, or the fifteenth, order, as compared to numerical results. The last trajectory, for $x_0 = y_0 = 2.8$, is chaotic. Thus, its series representation is no longer useful.

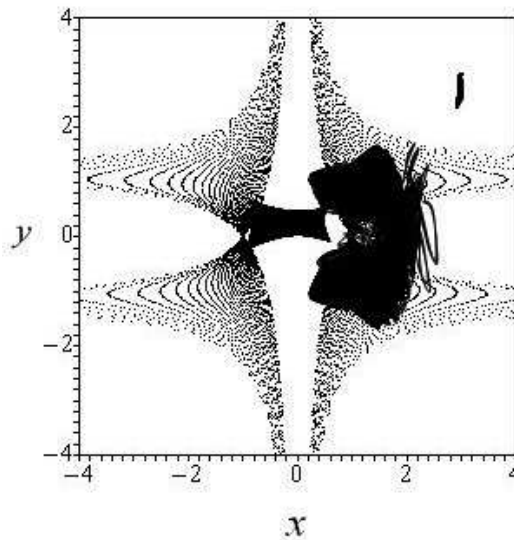


Figure 5. An ordered orbit in the inner regular domain (initial conditions $x_0 = y_0 = 0.5$), a chaotic orbit ($x_0 = y_0 = 1.5$), and an ordered orbit in the outer regular domain ($x_0 = y_0 = 3.0$) of the 2D harmonic oscillator model. The trajectories are plotted on top of the nodal lines.

results become appreciable. In fact, the trajectories of these initial conditions are still ordered and perform simple oscillations, although the analytical curves by the series expansions undergo large deviations. The level of approximation, as we decrease x_0, y_0 , can be judged from Table I yielding the analytical maxima and minima of the oscillating functions $x(t)$ and $y(t)$ as derived from the series truncated at orders $n = 4$ and $n = 15$. These numbers are compared with the limits of the trajectories found numerically. In all cases we take $a = b = 1$, $c = \sqrt{2}/2$. For $x_0 = y_0 \geq 3$ the agreement of both the 4th and 15th order approximations with the numerical results is very good.

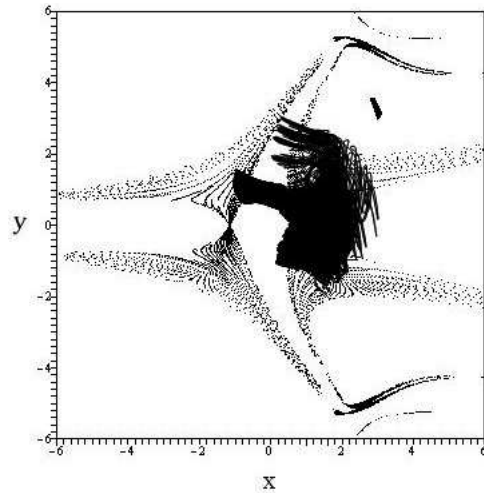


Figure 6. Same as in Fig.5, but for the Hénon-Heiles model.

On the other hand, for x_0, y_0 smaller than $\simeq 2.9$ (but not smaller than 1) the trajectories come into the domain of the nodal lines (Fig.5) and the trajectories become chaotic. This result shows that the chaotic trajectories are limited in a region covered by nodal lines (and even then some trajectories are still ordered if they do not approach the nodal points, as we have seen in the previous section).

5. Ordered trajectories in the Hénon - Heiles system

The main features of the quantum trajectories in the 2D harmonic oscillator model are maintained to a large extent if we consider perturbations of this model. Such perturbations present particular interest in various physical contexts ranging from molecular dynamics to quantum field theory.

As a simple nonlinear extension of the 2D harmonic oscillator model we consider the case of the Hénon - Heiles Hamiltonian

$$H = \frac{1}{2}(p_x^2 + \omega_1^2 x^2) + \frac{1}{2}(p_y^2 + \omega_2^2 y^2) + \epsilon x(y^2 - \frac{1}{3}x^2) \quad (28)$$

As in [18], we consider the case $\omega_1 = 1$, $\omega_2 = \sqrt{2}/2$, $\epsilon = 0.1118034$.

In order to compute a wavefunction in the above model which, as in the case of the wavefunction (4) of the 2D harmonic oscillator model, is the sum of the ground state and two states with quantum numbers (1,0) and (1,1), we first compute a 200×200 truncation of the Hamiltonian matrix of (28) using the basis functions of the 2D harmonic oscillator. The matrix elements considered are given by

$$H_{ij} = \int_{-\infty}^{\infty} \int_{-\infty}^{\infty} \phi_i(x, y) \hat{H} \phi_j(x, y) dx dy \quad (29)$$

where \hat{H} is the Hamiltonian operator corresponding to (28) expressed in the position representation, while $\phi_i(x, y)$ is the i -th eigenstate of the 2D harmonic oscillator model in the same representation. The index i is related to the 2D harmonic oscillator quantum

numbers (n, m) according to the bijective relation $i = m + 1 + (n + m)(n + m + 1)/2$. Thus, the i -th eigenvalue of the Hamiltonian (28) satisfies the relation $E_i = (n + 1/2) + (\sqrt{2}/2)(m + 1/2) + O(\epsilon)$. By diagonalizing the truncated real symmetric matrix \hat{H}_{tr} , with entries H_{ij} , $i, j = 1, 200$, we find the eigenvalues E_i and the corresponding normalized eigenvectors $\Phi_i(x, y)$, given by

$$\Phi_i = \sum_{j=1}^{200} c_j^{(i)} \phi_j(x, y) \quad (30)$$

where $c_j^{(i)}$, $j = 1, 200$ are the entries of the i -th column of the orthogonal diagonalizing matrix C satisfying $C \cdot H_{tr} \cdot C^{-1} = \text{diag}_{i=1}^{200}(E_i)$. Using the fact that the relation $i(n, m)$ is bijective, for ϵ sufficiently small we can assign quantum numbers to the i -th state of the Hénon-Heiles system via the inverse functions $n(i)$, $m(i)$. Using the above procedure, the eigenvalues and eigenstates up to $n, m = 2$ are computed with an estimated precision of six significant figures. Furthermore, we denote by $\Phi_{n,m}$ and $E_{n,m}$ the state $\Phi_{i(n,m)}$ as given by Eq.(30) and the corresponding eigenvalue $E_{i(n,m)}$ respectively.

In order, now, to make a comparison of the de Broglie - Bohm trajectories in the harmonic oscillator and in the Hénon - Heiles system, we study the trajectories under the wavefunction

$$\Psi(x, y, t) = e^{-iE_{0,0}t} \Phi_{0,0}(x, y) + a e^{-iE_{1,0}t} \Phi_{1,0}(x, y) + b e^{-iE_{1,1}t} \Phi_{1,1}(x, y) \quad (31)$$

We have examined various values of the real parameters a, b , as in the case of the 2D harmonic oscillator model.

Figure 6 shows an example of three Bohmian trajectories in the above model, i.e. (i) an inner ordered, (ii) a chaotic, and (iii) an outer ordered trajectory. This figure compares quite well with the corresponding figure for the 2D harmonic oscillator model (Fig.5), showing that ordered Bohmian trajectories persist even for perturbed hamiltonians of the form (28). In fact, by plotting also the nodal lines (gray in Fig.6), we note that they represent, to a large extent, a deformation of the nodal lines appearing in the respective figure (Fig.1) for the 2D harmonic oscillator model. In fact, the only noticeable difference concerns the right part of the (x, y) square in Fig.(6), for large (positive or negative) values of y and $x > 0$. Namely, while the nodal lines in Fig.5 tend to an asymptote at $x = 0$ for large y , the nodal lines in Fig.6 form two nearly horizontal zones at $y \approx \pm 4.5$. This, however, can only affect trajectories very far from the center (i.e. corresponding to an exponentially small probability), while the main form of the trajectories, as shown in Fig.6, follows the same features as analyzed in sections 3 and 4 for the 2D harmonic oscillator model.

6. Effects on quantum relaxation

The theory of *quantum relaxation*, introduced by Valentini [40], provides an extension of ordinary quantum mechanics leading to interesting physical consequences both for quantum particles [40][43][18][1][39] as well as quantum fields [6][5]. Briefly, the theory explores the consequences of allowing the possibility that a set of initial conditions of de

Broglie - Bohm trajectories have an initial probability density ρ_0 deviating from the one postulated by Born's rule i.e. $\rho_0 = |\psi_0|^2$, where ψ_0 is the initial wavefunction. The main result, called 'sub-quantum H-theorem' [40] predicts that on a coarse-grained level ρ can only approach closer to $|\psi|^2$ asymptotically in the forward sense of time (if $\rho_0 \neq |\psi_0|^2$), provided that the initial state has no 'fine grained micro-structure', i.e. ρ has initially no great fluctuations on very fine scales (see [40] for more precise definitions). Under such conditions, Valentini defines an H-function

$$H = \int dq \bar{\rho} \ln(\bar{\rho}/|\psi|^2) \quad (32)$$

where $\bar{\rho}$ is the average particle's density in cells produced after a choice of coarse-graining in configuration space, and $|\psi|^2$ is the average value of the square-modulus of the wavefunction in the same cells. It can be shown that H satisfies the inequality $H(t) - H(0) \leq 0$, but we emphasize that this does *not* imply that $H(t)$ is a monotonically decreasing function in time. Furthermore, it is possible to construct states such that $H(t) \simeq 0$ even if $\bar{\rho}$ differs significantly from $|\psi|^2$ from cell to cell, since the integrand in (32) can be both positive or negative. However, simulations indicate that the quantum relaxation is a numerical fact in several cases. In subsequent calculations, we probe directly the approach of ρ to $|\psi|^2$ on the basis of an alternative indicator, namely the integral of the absolute difference $|\rho - |\psi|^2|$ over the whole configuration space (see below), discussing also the relevance of this test to tests based on the temporal behavior of the H-function.

The interest in the quantum-relaxation theory is twofold: i) it provides a dynamical basis for deriving (rather than postulating) Born's rule, and ii) it leads to interesting new physics if we consider that fluctuations from Born's rule have a considerable amplitude during the early stages of evolution of particular quantum systems. A specific implementation regards the dynamical behavior of quantum fluctuations in the early Universe [34][42]. In fact, it was found [42] that if there were deviations from *quantum equilibrium* (i.e. Born's rule) in the early Universe, these could have led to detectable imprints in some observables encountered in the framework of physical cosmology (e.g. in the CBR spectrum).

Concrete numerical simulations of the relaxation mechanism were produced in [43], [18], and [39]. In all cases, it was found that the rate at which the phenomenon occurs depends on the existence of *chaotic* quantum trajectories, due to the appearance of *quantum vortices*, i.e. one or more vortex structures of the quantum flow. On the other hand, in [18] we noted that the presence of *ordered* trajectories suppresses quantum relaxation. Here, we explore this phenomenon in greater detail, but we also give an example of a rather surprising phenomenon, namely that quantum relaxation can be suppressed even in some cases of ensembles of chaotic rather than regular trajectories.

Figures 7,8,9 show the basic result. Figure 7 shows first a 'test' case, in which we compute the Bohmian trajectories of 961 (=31×31) trajectories in the 2D harmonic oscillator model (4), with $a = b = 1$, $c = \sqrt{2}/2$. The initial conditions are chosen by a rejection algorithm (see [35]) so as to provide a discrete sampling of an initial density

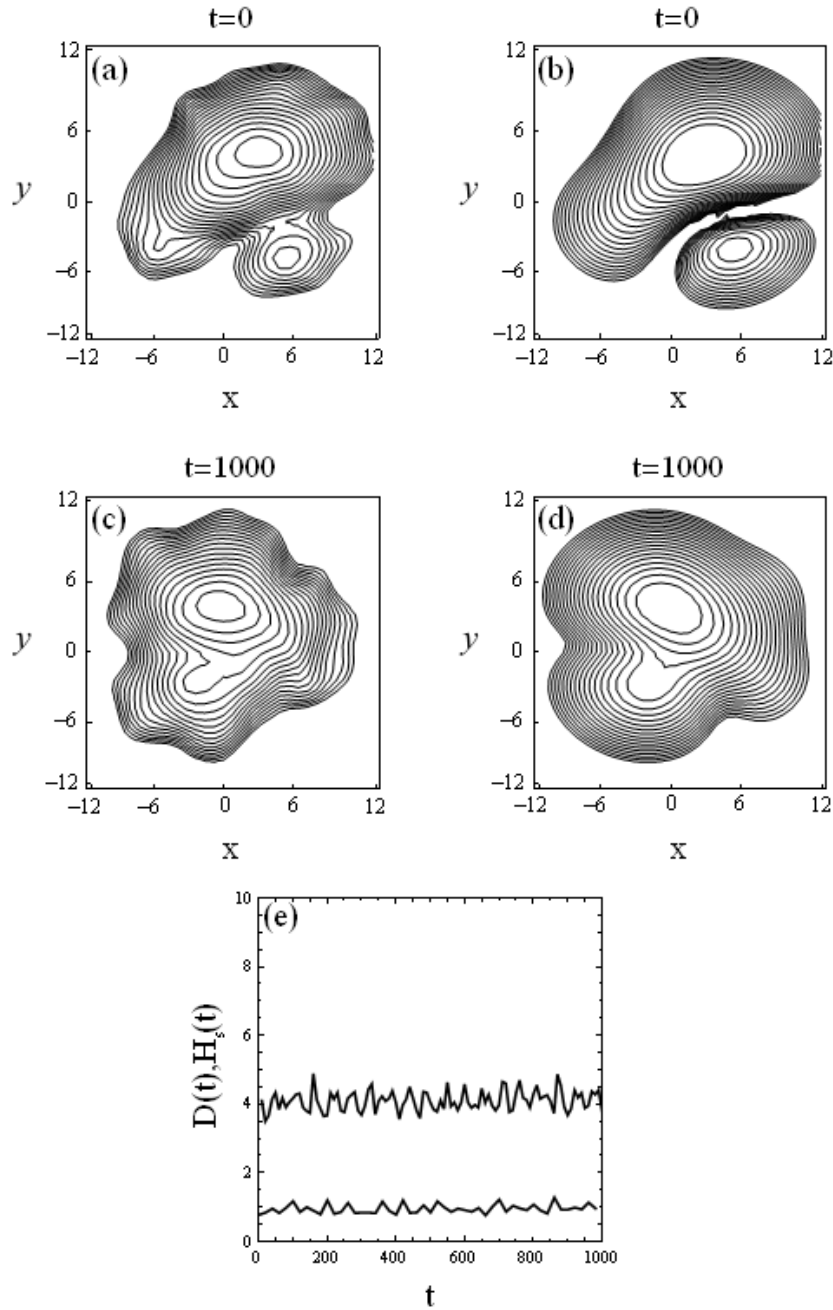


Figure 7. (a) The contour plots of the density $P_s(x, y, t)$ in a test case, where 961 particles are given initial conditions so as to represent a discrete realization of the probability $|\psi|^2$ given by Eq.(4) for $t = 0$. (b) Contour plots of the exact density $\rho = |\psi|^2$ at $t = 0$. (c) and (d) Same as in (a) and (b), but for $t = 1000$. The particles positions are now given by evolving their quantum trajectories. (e) Time evolution of the density difference $D(t)$ (upper curve) and of the H-function $H_s(t)$ (lower curve) in the same simulation.

distribution $\rho_0 = |\psi_0|^2$. We consider a relatively small number of particles (of order 1000) because we require that their trajectories should be subsequently computed by a small (and hence time-consuming) timestep $\Delta t = 10^{-4}$. This is needed in order to guarantee that no spurious numerical effects are introduced at least for the *regular* trajectories, which are our main concern here. In fact, for some trajectories we checked the results with a fixed timestep against an integration with variable time step supplemented by a regularization scheme when the distance from a nodal point becomes smaller than unity, as developed in [20], and found that both integrations are consistent.

The above limitation regarding the number of particles notwithstanding, we can compute a smooth approximation of the coarse-grained density sampled by these trajectories via the formula used in [18]:

$$P_s(x, y, t) = \sum_{i=1}^{961} A \exp \left[\frac{(x - x_i(t))^2 + (y - y_i(t))^2}{2\sigma^2} \right] \quad (33)$$

where σ is a Gaussian smoothing length, set equal to $\sigma = 0.3$. The constant A is computed so that the integral of the function $P_s(x, y, t)$ over the whole configuration space is equal to unity. Figures 7a,b display a comparison of the contour plots of the density $P_s(x, y, 0)$ (Fig.7a) and of $|\psi(x, y, 0)|^2$ (Fig.7b), showing that, by this choice of initial conditions, P_s turns to approximate fairly well the density $|\psi(x, y, 0)|^2$. The degree of approximation can be judged by computing (in time) an overall absolute density difference measure $D(t)$ in a grid of points, given by

$$D(t) = \sum_{k=1}^N \sum_{l=1}^N \left| P_s(x_k, y_l, t) - |\psi(x_k, y_l, t)|^2 \right| \quad (34)$$

where, as in [18], we set $N = 128$ and $x_k = -N/10 + k/5, y_l = N/10 + l/5$ in the sum (34). The initial value of this quantity for the above sample of orbits turns to be $D(0) \simeq 4$. As shown in [18], such a value is compatible with Poisson noise deviations of $P_s(0)$ from $|\psi_0|^2$, i.e. the two distributions are equal to within statistical fluctuations. Now, since the time evolution of the density resulting from a set of Bohmian trajectories should respect the continuity equation, as we evolve the Bohmian trajectories we should find this equality being preserved at all times t . This is indeed observed by a comparison of the contour plots of P_s and $|\psi|^2$ at subsequent times, as in Figs.7c,d, where this comparison is shown for the time $t = 1000$. The time evolution of $D(t)$ up to $t = 1000$ is displayed in Fig.7e, showing that $D(t)$ remains stuck at the statistical noise level $D(t) \simeq 4$, i.e. no significant deviations of P_s from $|\psi|^2$ develop as the numerical integration of the Bohmian trajectories proceeds in time. In the same plot, we show the behavior of the function

$$H_s(t) = \sum_{k=1}^N \sum_{l=1}^N P_s(x_k, y_l, t) \log \left(P_s(x_k, y_l, t) / |\psi(x_k, y_l, t)|^2 \right) \quad (35)$$

which is similar to Valentini's coarse-grained H-function computed over a coarse-graining at a resolution scale $\sim \sigma$. In fact, in the present as well as in all subsequent examples, we find that the two functions $D(t)$ and $H_s(t)$ have a quite similar temporal behavior.

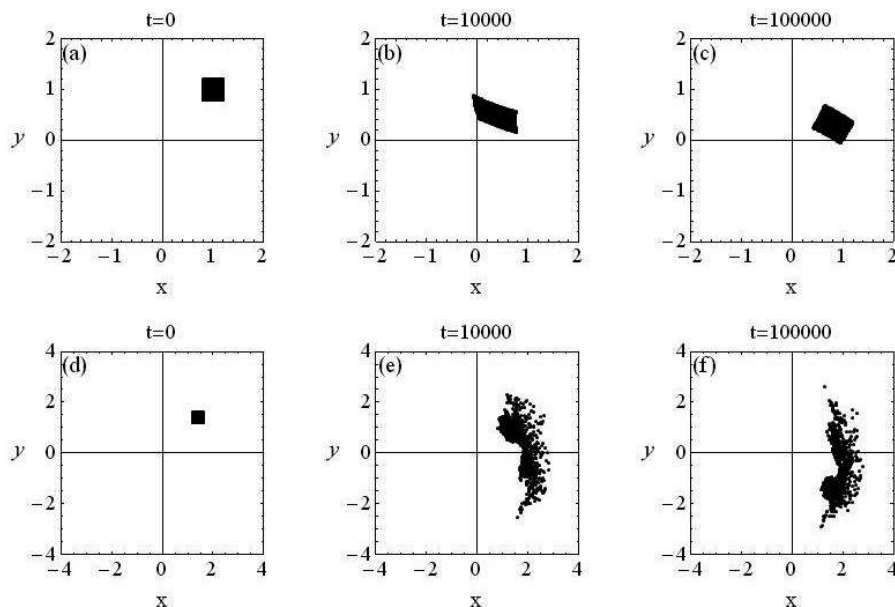


Figure 8. (a) The initial conditions of 961 particles in the ‘ordered’ ensemble of quantum trajectories considered for relaxation effects (see text) in the model of Eq.(4). (b),(c) Positions of the same particles at the times $t = 10000$ and $t = 100000$ respectively. (d),(e),(f) Same as in (a),(b),(c), but for a ‘chaotic’ ensemble of quantum trajectories.

This is because our way to choose initial conditions localized in small boxes implies that the main contribution to the sum (35) comes from cells (labeled by (k, l)) where one has $P_s > |\psi|^2$, whence it follows that

$$P_s \log(P_s/|\psi|^2) = P_s - |\psi|^2 + O[P_s(P_s/|\psi|^2 - 1)^2] .$$

We stress that, while this alternative calculation aims to approximate numerically the temporal behavior of the coarse-grained H-function, the most direct numerical test of the closeness of ρ to $|\psi|^2$ is provided by the numerical value of the quantity $D(t)$.

Figure 8, now, shows what happens if, instead, we start with initial conditions such that $P_s \neq |\psi|^2$. Figures 8a,b,c show the instantaneous positions at the times $t = 0$ (Fig.8a), $t = 10000$ (Fig.8b) and $t = 100000$ (Fig.8c), of 961 trajectories with initial conditions taken in a uniform 31×31 grid in the square box $(0.9, 1.1) \times (0.9, 1.1)$, in the same 2D harmonic oscillator model as in Fig.7. The central trajectory with initial conditions $x_0 = y_0 = 1$ is regular (Figure 1a). The same holds true for all its surrounding trajectories in the square. In Figs.8a,b,c it is then observed that the trajectories travel all together without any phase mixing taking place. As a result, the square area formed by this grid moves coherently from one to another domain of the configuration space, without exhibiting any systematic stretching or contracting along particular directions. This behavior is due to the fact that the numerical trajectories are found to exhibit quasi-periodic oscillations with two incommensurable frequencies which are the same for all the trajectories, namely $\omega_1 = 1$, and $\omega_2 = c$. In fact, this behavior is also

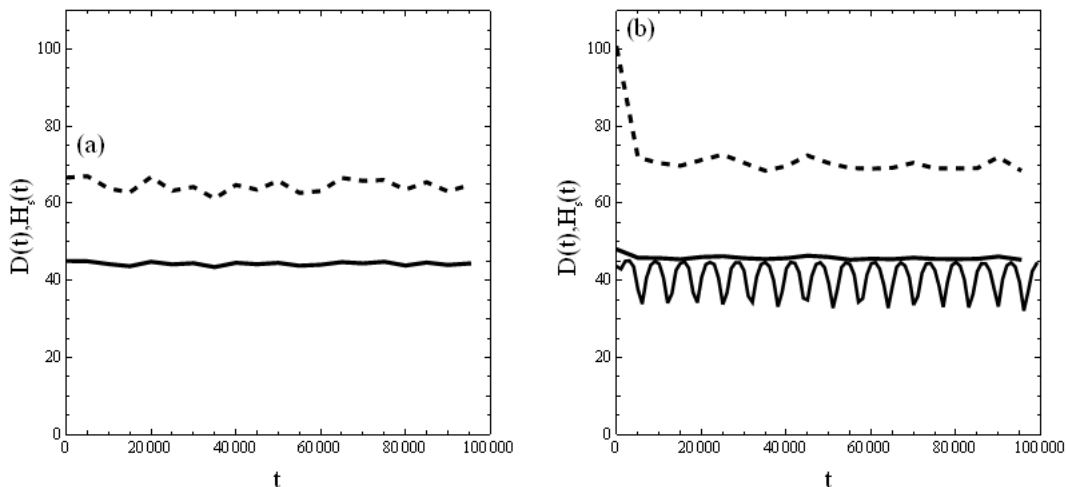


Figure 9. The time evolution of the density difference $D(t)$ (solid curve) and of the coarse-grained H-function $H_s(t)$ (dashed curve) for the ensemble of (a) the upper panels and (b) the lower panels of Fig.8. The lower oscillatory curve in (b) refers to a calculation of $D(t)$ in only the right semi-plane $x > 0$, denoted by $\bar{D}(t)$.

suggested by the series solutions of perturbation theory found for smaller values of a , and b , which share the same property. As a result, no phase mixing is possible for such trajectories.

Figures 8d,e,f show now a similar calculation for 961 trajectories with initial conditions in the square box $(1.3, 1.5) \times (1.3, 1.5)$. In this case, the central trajectory ($x_0 = y_0 = 1.4$) as well as all surrounding trajectories are chaotic. We now see that the trajectories expand in a considerable domain on both sides of the x-axis, however they always reside in the *same semi-plane* (i.e. right) with respect to the y-axis, i.e. the orbits never cross the y-axis. The no-crossing of the y-axis is due to the central gap formed between the innermost hyperbola-like limit of the nodal lines on both sides of the y-axis (cf. Fig. 1) The presence of such limits was shown theoretically in EKC. In fact, we have integrated some representative trajectories in the same sample up to a time $t = 10^5$, using a precise time step ($\Delta t = 10^{-4}$), and no hint of crossing of the y-axis was observed for any of them.

The fact that there can be chaotic trajectories limited within only a sub-domain of the total available configuration space implies that obstructions to quantum relaxation can be present even under chaotic de Broglie - Bohm dynamics. This is shown in Fig.9, showing a comparison of the evolution of $D(t)$ (Eq.(34)) for (a) the set of regular trajectories (upper panels in Fig.8), and (b) the set of chaotic trajectories (lower panels in Fig.8). In the case of regular trajectories (Fig.9a), we find that $D(t)$ undergoes small oscillations around a mean value $D(t) = 45$. This is consistent with the fact that ordered trajectories suppress quantum relaxation. However, the *same* trend is observed in the case of the chaotic trajectories, as shown in Fig.9b, since these trajectories never fill the

left semi-plane $x < 0$.

In this case also the value of $D(t)$ undergoes small oscillations around $D(t) \simeq 45$, and it does not tend to $D(t) = 0$ as t increases. But it should be pointed out that important deviations of P_s from $|\psi|^2$ are observed even if we limit ourselves to considering the sum (34) taken only on the semi-plane $x > 0$ (in this case we normalize both P_s and $|\psi|^2$ so that the surface integral of both quantities over the semi-plane $x > 0$ is equal to unity). We observe now that the new curve (denoted by $\overline{D}(t)$) undergoes oscillations, starting from a value $\overline{D} = 45$ and falling at particular moments down to $\overline{D} = 35$. Such trend is, however, subsequently reversed, and there are many cycles of rise and fall of $\overline{D}(t)$, but $\overline{D}(t)$ does not tend to zero.

A qualitative explanation of this behavior is provided by noting that the form of the wavefunction (4) allows for a recurrent transfer of quantum probability mass from the right to the left semi-plane and vice-versa. However, the considered ensemble, of only chaotic trajectories, contains no trajectories accounting for such transfer, i.e. no trajectories oscillating from one semi-plane to the other, but this transfer is only achieved in ensembles containing regular trajectories. Thus, despite the fact that we have chaotic trajectories, in this example P_s cannot tend to $|\psi|^2$ as t increases. We emphasize that this phenomenon occurs despite the fact that the wavefunction in the present case contains no disjoint supports. On the other hand, if there are two or more disjoint supports of the wavefunction, if we take initial conditions in only one support, relaxation never occurs even if all the trajectories are chaotic, since such trajectories cannot pass from the domain of one support to that of another at any later time t .

7. Further examples of obstruction to relaxation. Quantitative estimates

7.1. Further examples

The examples treated in sections 2 and 5 are rather special because even the chaotic trajectories are restricted on parts only of the total available configuration space. But we can construct other examples of mixed (i.e. co-existing regular and chaotic) dynamics where such restriction no longer holds. One such case is provided by the wavefunction model [20]:

$$\psi(x, y, t) = e^{-\frac{x^2+cy^2}{2}} e^{-\frac{1+c}{2}it} \left[1 + a(x^2 - 1)e^{-2it} + bc^{1/2}xye^{-it} \right] \quad (36)$$

for a, b, c real. Below, we choose $a = 1.23$, $b = 1.15$, $c = \sqrt{2}/2$. In [20] it was shown that this model contains both ordered and chaotic orbits. Figure 10 shows a calculation of two distinct sets of 961 trajectories each taken with initial conditions inside a 0.4×0.4 box centered at i) $x_0 = -1.5$, $y_0 = 0.1275$ and ii) $x_0 = -1.23$, $y_0 = 0.84$. The central values (i) and (ii) correspond to a regular and a chaotic orbit respectively. The main remark concerns the fact that, as is the case of regular orbits of the model of sections 2,3, and 5, the regular orbits in the present model undergo no phase mixing as well, i.e. they all do quasi-periodic oscillations with the frequencies $\omega_1 = 1$ and $\omega_2 = c = \sqrt{2}/2$. Furthermore, the boundary of the area occupied by the regular trajectories cannot

be penetrated by chaotic orbits. This effect is shown in Fig.10a depicting the initial conditions of the ordered and chaotic sets at $t = 0$, and their images at $t = 10000$, i.e. a time after which the chaotic trajectories spread over most of their allowable space belonging to the support of the system's wavefunction, while the ordered trajectories remain inside the black box.

Figure 10b shows the relaxation plots for the ensembles (i) and (ii) respectively. In the case of the ensemble (i) (regular orbits), we notice the clear deviation from relaxation, while in the case of the ensemble (ii) (chaotic orbits), both curves $D(t)$ and $H(t)$ approach a limiting mean value $D \simeq 12.3$, and $H_s \simeq 6.4$. In fact, we notice (Fig.10a) that the chaotic trajectories do not penetrate the boundary (closed gray curve) corresponding to the set of regular trajectories, thus, while $|\psi|^2$ covers all available space, the value of $\rho(t)$ is close to zero at all times within the domain delimited by this boundary. By calculating the percentage of the area occupied by regular orbits, versus the total area where all the orbits spread, we then estimate that the values reached by $D(t)$ and $H(t)$ on average show the expected difference from the 'noise' threshold indicating complete relaxation, which, in this case, is found to be $D = 9.9$ and $H_s = 4.4$ respectively.

Similar phenomena are found if we consider a superposition of four eigenfunctions

$$\begin{aligned} \psi(x, y, t) = & e^{-\frac{x^2+cy^2}{2}} e^{-\frac{1+c}{2}it} \\ & \times \left[1 + a(x^2 - 1)e^{-2it} + bc^{1/2}xye^{-i(1+c)t} + dx e^{-it} \right] \end{aligned} \quad (37)$$

with $a = b = d = 1$, and $c = \sqrt{2}/2$ (Figure 11). In fact, in this case, the domain occupied by regular orbits is numerically found to be larger than in the case of the wavefunction model (36) which is the superposition of a smaller number of states. In general, there appears to be no simple rule yielding the extent of the domain of regular orbits as the number of superposed eigenfunctions increases.

In systems like the 2D harmonic oscillator (Eq.(3) with c rational), or in the case of the square box examined e.g. in [43], the following property can be readily shown to hold true: an arbitrary combination of any number of eigenfunctions with real amplitudes implies that all motions are periodic (see [9]). In such systems, $D(t)$ and the coarse grained H-function are both periodic functions of time i.e. we have $D(T) = D(0)$ and $H(T) = H(0)$, where T is the period. One dimensional periodic models exhibiting the same effect were considered in [41]. In fact, this criterion can be used as a test of the accuracy of numerical integrations, i.e. by checking the periodicity of the numerically computed functions $D(t)$ or $H(t)$ in a periodic model.

If, now, the frequency ratio c in the Hamiltonian (3) is irrational, $H(t)$ has no periodic behavior. However, there can still be defined approximate periods by considering, for example, the rational truncates q_n/p_n of the continued fraction representation of the frequency ratio $c = \omega_2/\omega_1$ (assuming, without loss of generality, $\omega_1 > \omega_2$, i.e.

$$\omega_2/\omega_1 = [a_1, a_2, a_3, \dots] = \frac{1}{a_1 + \frac{1}{a_2 + \frac{1}{a_3 + \dots}}} \quad (38)$$

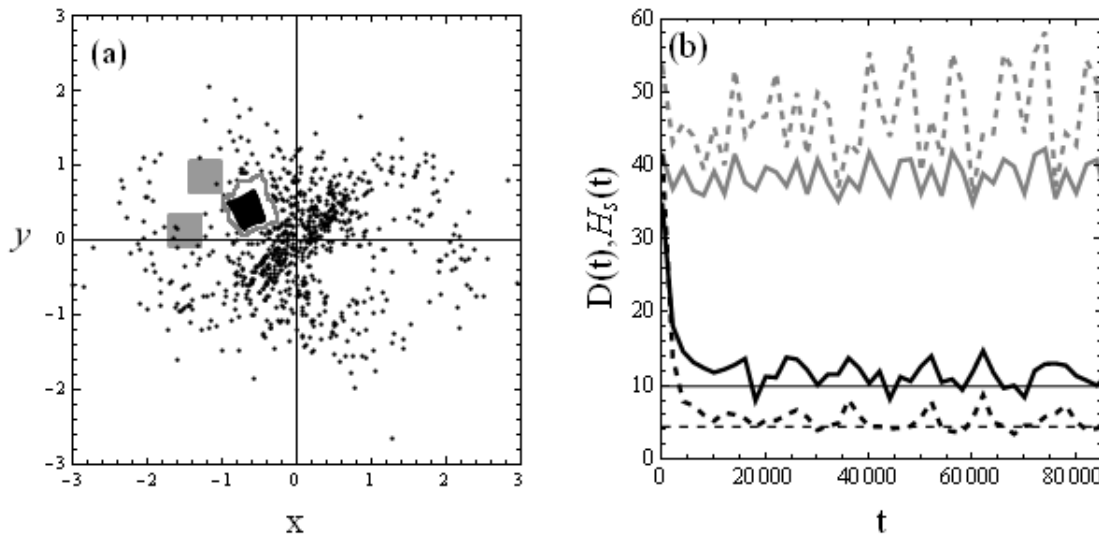


Figure 10. (a) The gray square boxes show the domains of initial conditions for a set of 961 trajectories in the wavefunction model (36), around the values (i) $x_0 = -1.5$, $y_0 = 0.1275$ (bottom square) and (ii) $x_0 = -1.23$, $y_0 = 0.84$ (up square). The black box contains the images of the points of the first box, at $t = 10000$, while the scattered points are the images of the points of the second box at the same time. The closed gray curve shows the approximate limit of the regular domain at the same time. (b) Time evolution of the quantities $D(t)$ (solid), and $H_s(t)$ (dashed) for the ensemble (i) (top curves, gray, regular trajectories), and (ii) (lower curves, black, chaotic trajectories). The straight solid line shows an average ‘noise’ level for $D(t)$ when we consider initial conditions satisfying $\rho_0 = |\psi_0|^2$. The curve $D(t)$ for the ensemble (ii) is, on average, a little above this level by a value $\Delta D \simeq 2.4$, which is consistent with a calculation taking into account the area left empty by the chaotic trajectories.

The n -th rational truncate, corresponding to the rational number $q_n/p_n = [a_1, \dots, a_n]$, defines an approximate period $T_n \approx 2\pi p_n/\omega_1$. Furthermore, for a large measure of incommensurable frequency pairs the following diophantine relation holds:

$$|q_n\omega_1 - p_n\omega_2| \approx \frac{\gamma}{q_n + p_n}$$

for a positive constant γ . On the other hand, the de Broglie-Bohm equations of motion can be written as combinations of odd trigonometric functions with arguments $(n_1\omega_1 + n_2\omega_2)t$. Then, using $\omega_1 = p_n\omega_2/q_n + O[1/(q_n(q_n + p_n))]$ and expanding the equations of motion we find that at the times $T_n \approx 2\pi p_n/\omega_1$ *all* trajectories are recurrent to nearly their initial positions to within an accuracy $O[2\pi/(p_n + q_n)]$. Since both q_n, p_n increase with n , we conclude that all trajectories come arbitrarily close to their initial conditions at very specific (and quite long, as n increases) times. This phenomenon can be considered as a quantum analog of the Poincaré recurrence for the de Broglie - Bohm trajectories.

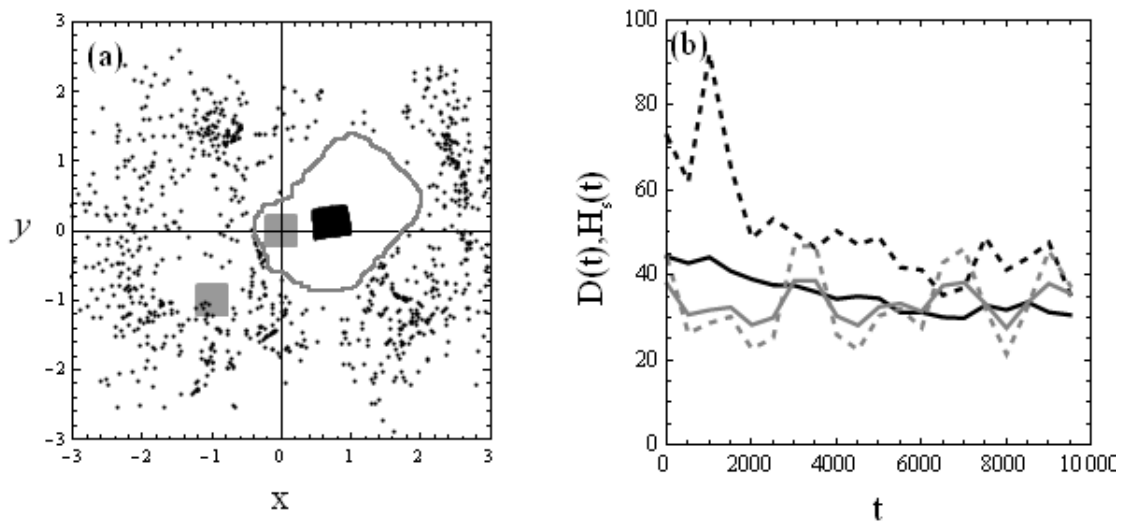


Figure 11. Same as in Fig.10, but for a superposition of four eigenfunctions (Eq.(37). In this case, the initial square boxes are centered around (i) $x_0 = y_0 = 0$ (regular trajectories), and (ii) $x_0 = y_0 = -1.1$ (chaotic trajectories). In (b) we note the large values of $D(t)$ and $H_s(t)$ for the chaotic ensemble as well, due to the fact that the chaotic trajectories are excluded from a large domain of the configuration space.

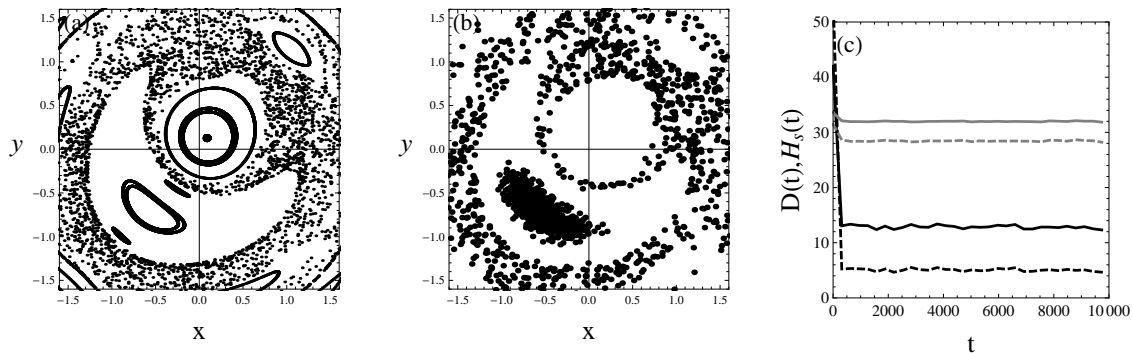


Figure 12. (a) Stroboscopic surface of section of the de Broglie - Bohm trajectories in the model (39) with $a = 0.17651$, $b = d = 1$, $\gamma_1 = 3.876968$, $\gamma_2 = 2.684916$, produced by taking the iterates up to $t = 5000$ of each one of 15 initial conditions along the diagonal $x = y$ from $x = y = -1.6$ to $x = y = 1.6$. (b) The iterates, at time $t = 2000\pi$, of a set of 961 initial conditions in a square box 0.2×0.2 centered at $x_0 = y_0 = -0.6$ (regular) remain constrained in the lower left island of stability, while the iterates of the initial conditions in a similar box around $x_0 = y_0 = 0.9$ (chaotic) fill a chaotic domain. (c) Time evolution of $D(t)$ (solid curves) and $H_s(t)$ (dashed curves) for the regular (top curves) and chaotic (lower curves) trajectories of (b).

7.2. Hamiltonian case (a, b complex)

The equality of the frequencies for all regular orbits is a particular property of the de Broglie - Bohm dynamics in systems with a superposition of three or more eigenfunctions

with a real amplitude. On the other hand, when the superposition amplitudes are complex rather than real, a novel feature may appear, namely we can construct particular combinations leading to a Hamiltonian representation of the de Broglie - Bohm equations of motion. In such cases the regular trajectories still exhibit quasi-periodic oscillations, but the frequencies are not fixed, i.e. they are not the same for all trajectories. However, obstructions to relaxation can still be posed by the appearance of *islands of stability* in the configuration space.

An example of this phenomenon is provided by the model considered in [45]:

$$\psi(x, y, t) = e^{-\frac{x^2+y^2}{2}} \left(ae^{-it} + bxe^{-2it-\gamma_1} + dye^{-2it-\gamma_2} \right) \quad (39)$$

with $a = 0.17651$, $b = d = 1$, $\gamma_1 = 3.876968$, $\gamma_2 = 2.684916$. The wavefunction (39) corresponds to a superposition of the states ψ_{00}, ψ_{10} and ψ_{01} in the Hamiltonian (3) with $c = 1$. In this particular case the de Broglie - Bohm equations of motion are given by a time-dependent Hamiltonian model [45], with period $T = 2\pi$, where y is equivalent to a momentum variable canonically conjugated to the position x . If we plot $x(t), y(t)$ along particular trajectories at the period multiples $t = 2\pi, 4\pi, \dots$, we obtain stroboscopic surfaces of section presenting typical features of a Hamiltonian system with mixed phase space. In Fig.12a we see this structure, which consists of the co-existence of several islands of stability surrounded by an intricate structure and chaotic layers. The key remark regarding relaxation is that the regular orbits cannot escape from the boundaries of the islands of stability. Thus, if we start with initial conditions exclusively in the domain occupied by one or more islands, the particles' coarse-grained density $\bar{\rho}$ always retains the value $\bar{\rho}(t) = 0$ in the chaotic domain of the configuration space, and vice versa, i.e. initial conditions in the chaotic domain lead to $\bar{\rho}(t) = 0$ inside the islands. This effect is shown in Fig.12b. The consequences for relaxation are shown in Fig.12c, where we observe that both quantities $D(t)$ and $H_s(t)$ remain far from zero for all times t up to $t = 10000$. We note that the regular trajectories inside an island (like the large lower left island in Fig.12a) exhibit a local phase mixing, which leads to a uniform distribution with respect to the angles after sufficiently long time. In fact, inside an island we can define a local form of an approximate integral of motion $I(x, y, t)$ (see [7]), i.e. a formal series in x, y with time-dependent trigonometric coefficients, whose formal time derivative, depending on the Poisson bracket with the Hamiltonian H , is given by an exponentially small estimate:

$$\frac{dI}{dt} = \frac{\partial I}{\partial t} + \{I, H\} = O(\exp(-1/r)) \quad (40)$$

where $r = [(x - x_0(t))^2 + (y - y_0(t))^2]^{1/2}$, and $(x_0(t), y_0(t))$ is the time evolution along the periodic orbit at the center of the island of stability (see [17] for a heuristic derivation of such estimates). This implies that, down to an exponentially small error, we can practically consider the invariant curves within an island of stability of Fig.12a as given by the level curves of $I(x, y, 0) = C$, for various values of the constant C . Then, it is straightforward to show that if we partition the configuration space within an island by considering a sequence of level values of the parameter C , then, independently of how

we partition the remaining configuration space, the coarse-grained H-function remains bound away from zero at all times t .

Finally, we should mention the cases of *coherent state* wavefunctions (see our work [18]), consisting of a superposition of infinitely many eigenfunctions, which exhibit no relaxation and contain only regular trajectories.

In view of the above examples, we conclude that order in de Broglie - Bohm quantum mechanics appears in a quite significant variety of contexts. On the other hand, in some other cases (e.g.[43][39]), using a larger number of eigenfunctions, relaxation effects were found to be complete. But in the case of exact or approximate coherent states, there can be all-time or finite-time obstructions to relaxation which, as found in [18] persist for times exponentially long in the inverse of a parameter (equivalent to the system's mean energy). The fact that such states are superpositions of infinitely many eigenfunctions shows that the number of eigenfunctions composing a particular quantum state cannot be used always as a good indicator of the speed of quantum relaxation. The issue of which particular superposition states speed up or slow down the relaxation process is interesting and is left for future research.

8. Conclusions

We examined the role of order in the de Broglie - Bohm approach to quantum mechanics, by studying the conditions for the existence of regular quantum trajectories, i.e. trajectories with a zero Lyapunov characteristic number. We found also a partial order even in some cases of chaotic trajectories. Finally, we studied the consequences of order in the phenomenon of quantum relaxation. Our main conclusions are the following:

1) We demonstrated, via low-order perturbation theory, that there are trajectories avoiding close encounters with the moving nodal points, in an example of a quantum state consisting of a superposition of three eigenfunctions in the 2D harmonic oscillator model. Due to this effect, there can be regular quantum trajectories extending spatially in a domain overlapping with the domain of nodal lines.

2) We computed series expansions for regular trajectories both in the interior and the exterior of the domain covered by nodal lines. We provided an estimate of the domains of the series convergence, and compared this with numerical trajectories. It was found that the series only provide a lower bound of the domains where regular trajectories are calculated by numerical means.

3) We examined the quantum trajectories in the Hénon - Heiles system, for quantum states similar to the ones used in the 2D harmonic oscillator models. The two cases yield a qualitative agreement as regards the extent of the domain and the initial conditions leading to regular trajectories. In the case of the Hénon - Heiles model, however, the nodal lines develop new structures leading to more chaotic trajectories.

4) We studied the influence of order in the so-called *quantum relaxation* effect, i.e. the approach in time of a spatial distribution ρ of particles following quantum trajectories to Born's rule $\rho = |\psi|^2$, even if initially $\rho_0 \neq |\psi_0|^2$. In previous works, it

was identified that chaos provides in general the dynamical substrate leading to the realization of Born's rule. Here, however, we show cases where the relaxation can be effectively suppressed when we consider ensembles not only of regular, but also of chaotic quantum trajectories. This is due to the fact that the existence of order in a system poses obstructions in the extent to which chaotic trajectories can mix in the configuration space. For the quantification of relaxation effects we compute two different quantities, namely a density difference $D(t)$ and an H-function $H_s(t)$ over a smoothed particle density P_s , and show that both quantities exhibit a similar temporal behavior.

5) We examined several models of superposition of a small number (three or four) of eigenfunctions and found that the existence of order in such models is generic. We also examined the case of complex superposition amplitudes, and explained how the appearance of islands of stability creates a new mechanism of obstruction of quantum relaxation. The degree of generality of the above phenomena is proposed as a subject for future study.

Acknowledgments: C. Delis was supported by the State Scholarship Foundation of Greece (IKY) and by the Hellenic Center of Metals Research. C.E. has worked in the framework of the COST Action MP1006 - Fundamental Problems of Quantum Physics.

References

- [1] Bennett, A.: 2010, *J. Phys. A* **43**, 5304.
- [2] Bohm, D.: 1952, *Phys. Rev.* **85**, 166.
Bohm, D.: 1952, *Phys. Rev.* **85** 194.
- [3] Bohm, D., and Vigier, J.P.: 1954, *Phys. Rev.* **96**, 208.
- [4] Bohm, D and Hiley, B.J.: 1993, *The Undivided Universe*, Routhledge, London.
- [5] Colin, S.: 2011, *arXiv1108.5496*.
- [6] Colin, S., and Struyve, W.: 2010, *New J. Phys.* **12**, 3008.
- [7] Contopoulos, G., 1960. *Z. Astrophys.* **49**, 273.
- [8] Contopoulos, G., and Efthymiopoulos, C.:2008, *Celest. Mech. Dyn. Astron.* **102**, 219.
- [9] Contopoulos, G., Efthymiopoulos, C., and Harsoula, M.: 2008, *Nonlin. Phenomena Com. Sys.* **11**, 107.
- [10] Cushing, J.T.: 2000, *Philos. Sci.* **67**, S432.
- [11] de Broglie, L.: 1928, in: J. Bordet (ed) *Electrons et Photons: Rapports et Discussions du Cinquième Conseil de Physique*, Gauthier-Villars, Paris.
- [12] de Sales, J.A., and Florencio, J.: 2003, *Phys. Rev. E* **67**, 016216.
- [13] Dewdney, C., and Malik, Z.: 1996, *Phys. Lett. A* **220**, 183.
- [14] Dirac, P.A.M.: 1931, *Proc. Royal Soc. London A*, **133**, 821, 60.
- [15] Durr, D., Goldstein, S. and Zanghi, N.: 1992, *J. Stat. Phys.* **68**, 259.
- [16] Dürr, D and Teufel, S: 2009, *Bohmian mechanics: the physics and mathematics of quantum theory*, Springer
- [17] Efthymiopoulos C, Giorgilli, A., and Contopoulos G.: 2004, *J. Phys. A: Math. Gen.* **37**, 10831.
- [18] Efthymiopoulos C., and Contopoulos, G.: 2006, *J. Phys. A* **39**, 1819.
- [19] Efthymiopoulos, C., Kalapotharakos, C., and Contopoulos, G.: 2007, *J. Phys. A* **40**, 12945.
- [20] Efthymiopoulos, C., Kalapotharakos, C., and Contopoulos, G.: 2009, *Phys. Rev. E* **79**, 036203.
- [21] Faisal, F.H.M., and Schwengelbeck, U.: 1995, *Phys. Lett. A* **207**, 31.
- [22] Falsaperla, P. and Fonte, G.: 2003, *Phys. Lett. A* **316**, 382.

- [23] Frisk, H.: 1997, *Phys. Lett. A* **227**, 139.
- [24] Garcia de Polavieja, G.: 1996, *Phys. Rev. A* **53**, 2059.
- [25] Hirschfelder, J., Christoph, A.C. and Palke, W.E.: 1974, *J. Chem. Phys.* **61**, 5435.
- [26] Hirschfelder, J., Goebel, C.J., and Bruch, L.W.: 1974, *J. Chem. Phys.* **61**, 5456.
- [27] Holland, P.: 1993, *The Quantum Theory of Motion*, Cambridge University Press, Cambridge.
- [28] Iacomelli, G., and Pettini, M.: 1996, *Phys. Lett. A* **212**, 29.
- [29] Konkel, S., and Makowski, A.J.: 1998, *Phys. Lett. A* **238**, 95.
- [30] Madelung, E.: 1926, *Z. Phys.* **40**, 332.
- [31] Makowski, A.J., Peplowski, P., and Dembinski, S.T.: 2000, *Phys. Lett. A* **266**, 241.
- [32] McCullough, E.A., and Wyatt, R.E.: 1971, *J. Chem. Phys.* **54**, 3578.
- [33] Parmenter, R.B., and Valentine, R.W.: 1995, *Phys. Lett. A* **201**, 1.
- [34] Peter, P., and Pinto-Neto, N.: 2008, *Phys. Rev. D* **78**, 063506.
- [35] Press, WH, Teukolsky, SA, Vetterling, WT, and Flannery, BP: 1986, *Numerical Recipes: The Art of Scientific Computing*. Cambridge University Press, New York.
- [36] Sanz, A.S., Borondo, F., and Miret-Artés, S: 2004, *J. Chem. Phys.* **120**, 8794.
- [37] Sanz, A.S., Borondo, F., and Miret-Artés, S: 2004, *Phys. Rev. B.* **69**, 115413.
- [38] Schlegel, K.G., and Forster, S.: 2008, *Phys. Lett. A* **372**, 3620.
- [39] Towler, M.D., Russell, N.J., and Valentini, A: 2011, arXiv1103.1589T.
- [40] Valentini, A: 1991a, *Phys. Lett.* **156**, 5.
Valentini, A: 1991b, *Phys. Lett.* **158**, 1.
- [41] Valentini, A H: 2001, "Hidden variables, Statistical Mechanics, and the Early Universe", *ArXiv: quant-ph/0104067v1*.
- [42] Valentini, A: 2010, *Phys. Rev. D* **82**, 063513. 253.
- [43] Valentini, A and Westman, H: 2005, *Proc. R. Soc. A* **461** 253.
- [44] Wu, H., and Sprung, D.W.L.: 1999, *Phys. Lett. A* **261**, 150.
- [45] Wisniacki, D.A., and Pujals, E.R.: 2005, *Europhys. Lett.* **71**, 159.
- [46] Wisniacki, D.A., Pujals, E.R., and Borondo, F.: 2007, *J. Phys. A* **40**, 14353.